# Structural model for pseudobinary semiconductor alloys

Matthias C. Schabel and José Luís Martins
*Department of Chemical Engineering and Materials Science, University of Minnesota, Minneapolis, Minnesota 55455*
(Received 29 November 1990)

Using the Keating valence-force-field model with large periodic supercells, we analyze the structural relaxations of pseudobinary III-V and II-VI semiconductor alloys. We quantitatively predict the dependence of bond lengths and second-neighbor distances on alloy composition, and show that the multimodal distributions of second-neighbor distances may be explained in terms of a simple set of local geometries. Intrinsic alloy broadening of bond-length distributions is also calculated and compared with experimentally measured values.

## I. INTRODUCTION

In regions of solid-solution miscibility, the properties of two constituent materials may be significantly varied as alloy composition changes.[1] This is particularly true in semiconducting systems such as the binary alloys of group-IV elements and pseudobinary alloys of III-V and II-VI compounds. For example, the composition-dependent band gap of $Si_xGe_{1-x}$ ranges from 0.66 to 1.11 eV with $x$. In the same manner, the wavelength at which a $Ga_xIn_{1-x}As_yP_{1-y}$ solid-state laser emits may be changed with composition. However, many alloy properties have a nonlinear dependence on composition which is difficult to predict quantitatively without accurate structural characterization.

Structural analysis of semiconductor alloys originated with x-ray diffraction experiments used to determine the crystal structure and the dependence of lattice constant on composition. These studies showed the formation of zinc-blende alloy crystals with a lattice constant varying linearly between the values of the end-point compounds[2] (Vegard's law). However, extended x-ray absorption fine structure (EXAFS) studies revealed a bimodal distribution of bond lengths in a number of these materials,[3–8] pointing to additional complexities in their local structure. This finding had significant ramifications for studies of electronic structure,[9,10] and spurred new interest in the distortions of atoms in pseudobinary alloys from their ideal zinc-blende positions.

The electronic properties of semiconductor alloys are altered by the existence of these atomic distortions. Models neglecting this, such as the virtual-crystal approximation (VCA) or the coherent-potential approximation (CPA) with strictly diagonal disorder, can only be applied to the relatively small number of alloys comprised of lattice matched constituents (e.g., $Al_xGa_{1-x}As$). To study the effects of relaxation, models using a local description of the alloy such as the molecular coherent-potential approximation[10] (M-CPA) or a periodic supercell approach[9] should be used. In the case of the latter, it has been recently argued that surprisingly small supercells represent the random alloy well if the most important site correlations of the infinite alloy are well duplicated by the periodic model.[11] These considerations make an understanding of structural relaxation and bond-length distributions in pseudobinary semiconductor alloys fundamental to studies of their electronic and thermodynamic properties.

Of current models giving a realistic description of the structural relaxation of semiconductor alloys, the valence-force-field (VFF) approach is the simplest. This model assumes that the energetics of atomic displacement can be accurately approximated in terms of a classical interatomic potential. Such an approach works well where distortions are small and there is no significant alteration of the bonding structure in the alloy. The Keating[12] valence force field has been previously applied to the study of alloy relaxation by several authors, providing results in general agreement with experimental data. However, with the exception of the finite cluster model of Podgòrny *et al.*[13] and Qteish, Motta, and Balzarotti,[14] these calculations limit relaxation to a few shells around an impurity[15,16] or assume zero relaxation of the mixed sublattice.[5,17]

Here we present a simulation of pseudobinary zinc-blende semiconductor alloys using the Keating VFF and a periodic cubic supercell geometry with 216 atoms. We provide results for the average first- and second-neighbor distances and first-neighbor distribution widths for eighteen III-V and eleven II-VI systems. We also explain the origin of multimodal distributions of second-neighbor distances in terms of a small number of components arising from specific configurations of neighboring atoms. Finally, we compare our results to available experimental data,[3–8] and show good agreement between the two.

## II. PROCEDURE

In our calculations of structure in pseudobinary zinc-blende structure alloys, the Keating valence-force-field (VFF) potential[12] was chosen because previous calculations[13–17] using this model show good correspondence with the available experimental results. In addition, this potential uses only three empirical parameters to describe the interactions in a tetrahedral semiconductor. For an arbitrary supercell containing $2N$ atoms ($N$ on each sublattice), the Keating potential is

 

$$U=\sum_{\langle ij\rangle}^{4N}\frac{3\alpha_{ij}}{8(R_{ij}^{0})^2}[\mathbf{r}_{ij}^2-(R_{ij}^{0})^2]^2 + \sum_{\angle ijk}^{12N}\frac{3\beta_{ijk}}{8R_{ji}^{0}R_{jk}^{0}}\left[\mathbf{r}_{ji}\cdot\mathbf{r}_{jk}+\frac{R_{ji}^{0}R_{jk}^{0}}{3}\right]^2, \quad (1)$$

where $R_{ij}^{0}$ is the equilibrium bond length between atoms $i$ and $j$ in the pure zinc-blende compound, $\mathbf{r}_{ij}$ is the vector between first neighbors, and $\alpha_{ij},\beta_{ijk}$ are empirical bond-stretching and bond-bending constants, respectively. Energy in the Keating model [Eq. (1)] is determined as the sum of two separate contributions. The first summation in Eq. (1) represents the contribution of bond-length compression or dilation to total energy while the second sum includes energy terms arising from distortion of bond angles from the ideal tetrahedral angle. Values for the constants $R_{ij}^{0}$, $\alpha_{ij}$, and $\beta_{ijk}$ for pure compounds are taken from the table of Martins and Zunger.[15] For heterogeneous bond angles, $\beta_{ijk}$ is estimated as the geometric mean of the bond-bending constants for the pure compounds: $\beta_{ijk}=\sqrt{\beta_{iji}\beta_{kjk}}$. It should be noted that this model uses empirical parameters determined from the elastic properties of the pure zinc-blende compounds, and does not use any additional unconstrained parameters or experimentally derived data to conform to experiment.

An infinite, random alloy lattice was simulated in our calculations using a zinc-blende supercell with periodic boundary conditions. The supercells were constructed as cubical lattices with $n$ conventional zinc-blende unit cells per side, corresponding to a cell in which each of the fcc sublattices is occupied by $N=4n^3$ atoms. In the present simulations the lattice constant of the alloy was assumed to be the concentration weighted average of the lattice constants of the pure end-point compounds.[2] Minimization of the energy in Eq. (1) with respect to alloy lattice constant was performed for several systems by calculating the average supercell total energy over a range of values of this parameter. In all instances the value of the lattice constant which provided a minimum differed insignificantly from the interpolated value, verifying the validity of our assumption. Consequently, for the sake of expediting calculations, all subsequent simulations used the alloy lattice constant predicted by Vegard's law.

In constructing the random $A_xB_{1-x}C$ supercell, points lying within the cell are separated into a mixed and an unmixed (common) sublattice, the former with a random distribution of atoms of types $A$ and $B$ and the latter occupied with atoms of type $C$. The composition of a simulated supercell assumes a finite number of possible values, determined by the number of atoms in each of the sublattices. For example, in a supercell of $A_xB_{1-x}C$ containing $2N$ atoms, $x$ varies from 0 to 1 in steps of $1/N$. The $Nx$ atoms of type $A$ are placed in unoccupied lattice sites randomly chosen from those in the mixed sublattice. Once these sites are allocated, the remaining mixed sublattice sites are filled with $N(1-x)$ type-$B$ atoms, and the common sublattice is uniformly occupied with $N$ atoms of type $C$. This method of site occupation simulates a random alloy with neither short- nor long-range chemical ordering. By allocating a constant number of atoms of type $A$ for each random cell configuration, the simulations are carried out at fixed composition. This contrasts with sampling over a grand-canonical ensemble in which chemical potential rather than occupation fraction is held constant.

For each random supercell configuration tested, we minimize energy [Eq. (1)] with respect to the atomic coordinates using a Broyden-Fletcher-Goldfarb-Shanno[18] conjugate gradient scheme. Within each randomly configured supercell having $N$ atoms on each fcc sublattice, there exist $4N$ first-neighbor bond lengths and $12N$ bond angles (equivalently second-neighbor distances). These quantities do not assume a single value uniformly throughout the cell. Instead they exist as a distribution about some mean which is dependent on the properties of the constituent compounds and the alloy composition. Each random reconfiguration of the cell at fixed composition provides a slightly different set of distributions; the properties of the ideal alloy are approximated as averages over $M$ different supercell configurations. Two sources of error occur in this calculation, the first stemming from the finite cell size and periodic boundaries, and the second arising from a finite number of samples over the configuration space. For 216-atom supercells in a cubic configuration, the boundaries will only enter into interactions involving the eighth- and more-distant-neighbor shells, so this effect is essentially negligible. For example, convergence of elastic energy with supercell size was determined for cells containing 8, 64, and 216 atoms at a composition $A_{0.5}B_{0.5}C$, with the two larger cells tested by averaging over 500 random cell configurations. For $Ga_{0.5}In_{0.5}As$, the energy per atom averaged over all configurations dropped from 1.26 to 1.18 mRy when the supercell size was increased from 8 to 64 atoms. Use of a larger cell with 216 atoms resulted in an insignificant increase in the energy of $1\times10^{-2}$ mRy/atom. From these values, it is clear that the error arising from our finite cell size is insignificant in comparison with the expected physical accuracy of the Keating model. In contrast, the error resulting from the limited number of samples in the space of cell configurations must be accounted for in any simulation of manageable size. In each calculation over $M$ configurations, we have a total of $4NM$ bond lengths and $12NM$ second-neighbor distances in the statistical sample of the distributions of these values. The error arising from this source, which decreases as $M^{-1/2}$, is quoted in our tabulated values except where it is smaller than the least significant digit given.

## III. RESULTS

Minimization of the total energy for each supercell configuration results in a set of relaxed atomic positions deviating from the ideal zinc-blende vectors. Measurement of the relative distortions of each sublattice (mixed and common) is accomplished by defining a sublattice distortion parameter

$$S=\min_{\mathbf{t}}\frac{1}{N}\sum_{i=1}^{N}(\mathbf{R}_i-\mathbf{p}_i-\mathbf{t})^2$$

$$=\frac{1}{N}\left[\sum_{i=1}^{N}(\mathbf{R}_i-\mathbf{p}_i)^2-\frac{1}{N}\left[\sum_{i=1}^{N}(\mathbf{R}_i-\mathbf{p}_i)\right]^2\right], \quad (2)$$

where $\mathbf{R}_i$ is the ideal zinc-blende lattice vector, $\mathbf{p}_i$ is the relaxed position of atom $i$, and the $\mathbf{t}$ which provides a minimum for the sum is $\mathbf{t}_0=(1/N)\sum_{i=1}^{N}(\mathbf{R}_i-\mathbf{p}_i)$. The introduction of the vector $\mathbf{t}$ allows for global translation of all sites in the sublattice from their original zinc-blende positions without additional distortion, ensuring translational invariance in the definition of $S$.

In Fig. 1 we present a graph of $S$ as a function of alloy composition for both the mixed and common sublattices of a $Ga_xIn_{1-x}As$ supercell, averaged over 500 random configurations. As observed previously,[4,13] the distortion of the common sublattice is consistently greater than that for the mixed sublattice at any given supercell composition. In addition, the distortion parameter for both sublattices is well described by a quadratic function of the form $S(x)\simeq 4S_0x(1-x)$. Some of the simplest alloy models assume zero distortion for the mixed sublattice;[5,17] i.e., $S^{(M)}=0$, restricting deviation from ideality to the common sublattice ($S^{(C)}\neq 0$). Clearly, as shown in the figure, $0<S^{(M)}\simeq\frac{1}{4}S^{(C)}$, revealing a small but nonnegligible distortion of the mixed sublattice. The EXAFS study of Mikkelsen and Boyce,[3,4] has shown that the average deviation of the common (As) sublattice in $Ga_xIn_{1-x}As$ from the ideal zinc-blende sites is significantly greater than that of the mixed (Ga,In) sublattice. The dichotomy in $S$ between the mixed and common sublattices is attributed to differences in local chemical environment. In particular, each cation in the mixed sublattice has a uniform neighborhood of As atoms on the tetrahedral bonding sites. This restricts inhomogeneities in the cation distribution to the second-neighbor and more distant shells. In contrast, each As atom on the common sublattice is surrounded by four cations, providing five possible distinct first-neighbor environments. Of these, three ($Ga_3In$, $Ga_2In_2$, and $GaIn_3$) lead to local distortion of the As atom from its zinc-blende site, assuming the absence of effects from shells beyond the second. As a consequence, variation in local environment affects the common sublattice to a measurably greater degree than the mixed sublattice.

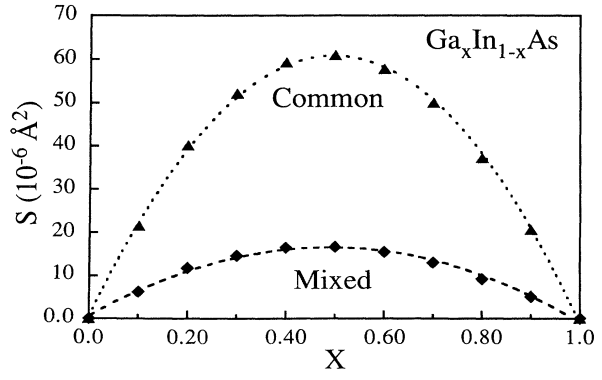


FIG. 1. The sublattice distortion parameter $S$, defined in Eq. (2), is plotted as a function of alloy composition $x$ for both the mixed and common sublattices of $Ga_xIn_{1-x}As$. Solid symbols represent calculated values, with a quadratic fit shown as the dashed curve.

While $S$ describes the overall relaxation of the individual sublattices, a more accurate picture of the structure of alloy supercells arises from analysis of the distributions of nearest-neighbor distances and next-nearest-neighbor distances. For any supercell configuration $C_i$ there will be distributions of these quantities representative of the infinite lattice associated with that supercell arrangement. Each distribution has a characteristic mean value $R_i$ and width $\Gamma_i$ for configuration $C_i$. When these values are averaged over the $M$ configurations, we obtain the final mean bond length $\bar{R}_{NN}$, second-neighbor distance $\bar{R}_{NNN}$, and the intrinsic distribution widths, $\bar{\Gamma}_{NN}$ and $\bar{\Gamma}_{NNN}$. For a random supercell of $A_xB_{1-x}C$ there are two distinct distributions of bond lengths, $(AC)$ and $(BC)$. There are also five distinct distributions of second-neighbor distances: $(ACA)$, $(BCB)$, $(ACB)$, $(CAC)$, and $(CBC)$, where $(ACB)$ is the distribution of NNN distances between atoms of type $A$ and $B$, with an atom of type $C$ at the vertex of the bond angle $\angle ACB$. Clearly, in and $A_xB_{1-x}C$ supercell containing $N$ atoms on each of the fcc sublattices, there will be $2Nx$ bonds of type $A$-$C$, and $2N(1-x)$ of type $B$-$C$. More generally, the binomial Bernoulli distribution gives the probability of finding $n$ atoms of type $A$ on $m$ sites, with an occupation fraction $x$ as $P(m,n,x)=\binom{m}{n}x^n(1-x)^{m-n}$. Using this expression for the second-neighbor distances, the relative numbers for each of these five distributions for a random supercell are $N_{ACA}=Nx^2$, $N_{BCB}=N(1-x)^2$, $N_{ACB}=Nx(1-x)$, $N_{CAC}=Nx$, and $N_{CBC}=N(1-x)$.

EXAFS measurements yield values for the first- and second-neighbor distances which may be directly compared to the $\bar{R}_i$'s calculated in our simulations. We compare calculations for $Ga_xIn_{1-x}As$ with the experimental EXAFS results of Mikkelsen and Boyce,[3,4] and present a detailed analysis of the structural behavior of this particular system. The data for $Ga_xIn_{1-x}As$ were obtained using 500 random configurations of the 216-atom supercell. Calculations were performed for thirteen values of $x$ in the range $Ga_{0.05}In_{0.95}As$ to $Ga_{0.95}In_{0.05}As$, providing average values and standard errors for $\bar{R}_{GaAs}$, $\bar{R}_{InAs}$, $\bar{R}_{Ga\text{-}As\text{-}Ga}$, $\bar{R}_{Ga\text{-}As\text{-}In}$, $\bar{R}_{In\text{-}As\text{-}In}$, $\bar{R}_{As\text{-}Ga\text{-}As}$, and $\bar{R}_{As\text{-}In\text{-}As}$.

Values for bond lengths in $Ga_xIn_{1-x}As$ calculated from the Keating model are compared with EXAFS results[3,4] in Fig. 2. The theoretical predictions for the Ga—As bond length lie within experimental error bars for the EXAFS data over the entire range of compositions. At small values of $x$, the predictions for the In—As bond also agree well with experimentally measured values. However, at large $x$, the results of our calculation overestimate the contraction of the In—As bond as compared to the EXAFS measurements. Agree-

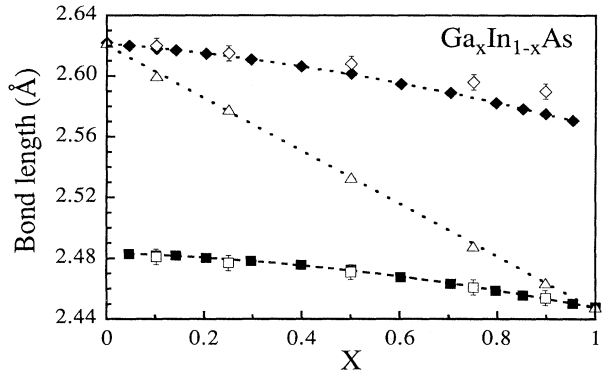


FIG. 2. Average Ga—As (squares) and In—As (diamonds) bond lengths for $Ga_xIn_{1-x}As$ are shown. Values taken from experimental EXAFS measurements (open symbols) are compared with the predictions of our model (solid symbols). X-ray diffraction measurements (open triangles) are superimposed with the linear interpolation between end-point values (dashed line).

ment with the EXAFS data could be improved by reducing the bond-bending constant, $\beta_{InAs}$, thus increasing the penalty for compressing the In—As bond relative to the penalty for bond bending. It has been argued that smaller values of $\beta$ better describe the overall phonon spectra of semiconductor alloys. However, while it is possible to better reproduce the experimental results by adjusting the value of this parameter, it is not the purpose of this work to fit the Keating constants to experimental data.

Figure 3 compares our calculations with the EXAFS measurements of second-neighbor distances for each of the five distinct NNN distributions. In the top panel, we see excellent correlation for both the As-Ga-As and Ga-As-In second-neighbor distances, with theoretical predictions lying within error bars for all data points. Again, predicted values of the As-In-As second-neighbor distances are lower near $x=1$, for the same reason that the calculated In—As bond lengths deviate from experiment. In the bottom panel we compare results for the Ga-As-Ga and In-As-In NNN distances, again revealing excellent correspondence between the two data sets. In the limit of the pure end-point compound, ($\bar{R}_{\text{Ga-As-Ga}}$,$\bar{R}_{\text{As-Ga-As}}$), and ($\bar{R}_{\text{In-As-In}}$,$\bar{R}_{\text{As-In-As}}$) approach the ideal second-neighbor distance as expected, while $\bar{R}_{\text{Ga-As-In}}$ exhibits relaxation at both extremes as should occur for a mixed second-neighbor distribution which exists as an impurity at both $x=0$ and 1. Additional support for our interpretation of the relative distortions of the two sublattices is provided by the behavior of these second-neighbor distances with composition. Examination of the mixed sublattice NNN distributions reveals a nearly linear dependence of $\bar{R}_{\text{NNN}}$ on $x$ between the end-point second-neighbor distances. In contrast, the NNN distances on the common sublattice both deviate strongly from the interpolated value as the impurity limit is approached. However, in both cases, a non-negligible distortion of the sublattice is indicated.

Additional EXAFS results[3–8,19] for $Ga_xIn_{1-x}P$, $InP_xAs_{1-x}$, $GaAs_xSb_{1-x}$, $Cd_xZn_{1-x}Te$, and $Cd_xHg_{1-x}Te$ are given in Table I along with values calculated from our model. Agreement between the two is good in most cases, with our calculated values lying within experimental error bars for all data except impurity Ga—Sb bond lengths in $GaAs_xSb_{1-x}$. For the latter, EXAFS data exhibit virtually no Ga—Sb bond-length relaxation, while we predict a relaxation of $\approx 0.06$ Å.

Analogous calculations were performed for all ternary III-V and eleven ternary II-VI alloys using $M=50$ random cell configurations for $A_xB_{1-x}C$, providing bond lengths and second-neighbor distances. These data were fitted with a quadratic polynomial in composition, providing parameters for a functional relationship between the $\bar{R}_i$'s and alloy composition, $x$. Table II presents the quadratic parameters, with standard errors, for the bond lengths in these compounds, with parameters and errors for second-neighbor distances provided in Tables III and IV. The pure $AC$ functions $\bar{R}_{AC}$, $\bar{R}_{ACA}$, and $\bar{R}_{CAC}$ are given as

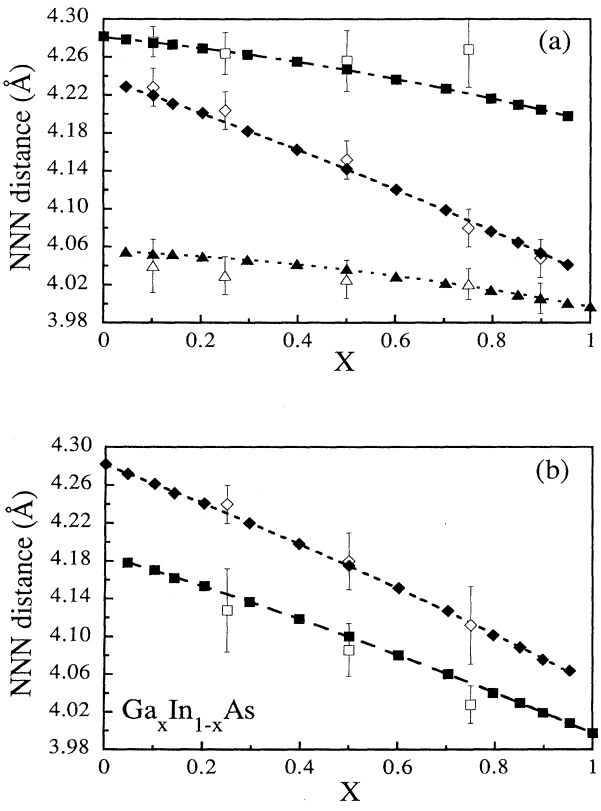


FIG. 3. Average NNN distances for $Ga_xIn_{1-x}As$ are shown as open symbols for experimental data and solid symbols for the predictions of our model. The top panel presents the As-In-As (squares), Ga-As-In (diamonds), and As-Ga-As (triangles) second-neighbor distances, fit with quadratic functions (dashed lines). The In-As-In (diamonds) and Ga-As-Ga (squares) results are shown in the bottom panel.

TABLE I. Comparison of experimental EXAFS data to predicted bond lengths.

| $A_xB_{1-x}C$ $CA_xB_{1-x}$ | $x$ | Experimental $R_{AC}$ (Å) | Experimental $R_{BC}$ (Å) | Predicted $\bar{R}_{AC}$ (Å) | Predicted $\bar{R}_{BC}$ (Å) |
|---|---|---|---|---|---|
| Ga-In-P[a] | 0.00 | 2.41±0.01 | | 2.399 | |
| In-P-As[a] | 1.00 | | 2.60±0.01 | | 2.602 |
| Ga-As-Sb[b] | 0.03 | 2.49±0.01 | 2.64±0.01 | 2.494 | 2.639 |
| | 0.05 | 2.47±0.01 | 2.64±0.01 | 2.493 | 2.638 |
| | 0.10 | 2.47±0.01 | 2.635±0.01 | 2.492 | 2.636 |
| | 0.90 | 2.45±0.01 | 2.62±0.01 | 2.455 | 2.585 |
| | 0.95 | 2.45±0.01 | 2.63±0.01 | 2.451 | 2.581 |
| Cd-Zn-Te[c] | 0.25 | 2.77±0.01 | 2.65±0.01 | 2.782 | 2.647 |
| | 0.50 | 2.785±0.01 | 2.66±0.01 | 2.792 | 2.654 |
| | 0.75 | 2.79±0.01 | 2.67±0.01 | 2.800 | 2.658 |
| Cd-Hg-Te[d] | 0.50 | 2.81±0.01 | 2.795±0.01 | 2.805 | 2.799 |

[a]Reference 8.
[b]Reference 14.
[c]Reference 5.
[d]Reference 19.

$$\bar{R}(x)=R^0+b(1-x)+c(1-x)^2 , \quad (3)$$

while distributions for $\bar{R}_{BC}$, $\bar{R}_{BCB}$, $\bar{R}_{CBC}$, and $\bar{R}_{ACB}$ are

$$\bar{R}(x)=R^0+bx+cx^2 . \quad (4)$$

These choices for the functional dependence on $x$ allow us to fit the theoretical data with the value of $R^0$ fixed for pure compounds, thus avoiding introduction of spurious errors in these parameters. For the mixed NNN distance $\bar{R}_{ACB}$, which exists as an impurity at both $x=0$ and 1, all three parameters will have intrinsic statistical errors. However, as the magnitude of the error in $\bar{R}^0_{ACB}$ is much

TABLE II. Quadratic parameters for bond lengths [Eqs. (3) and (4)].

| $A_xB_{1-x}C$ $CA_xB_{1-x}$ | $\bar{R}_{AC}[f(1-x)]$ $R^0$ (Å) | $b$ ($10^{-3}$ Å) | $c$ ($10^{-3}$ Å) | $\bar{R}_{BC}[f(x)]$ $R^0$ (Å) | $b$ ($10^{-3}$ Å) | $c$ ($10^{-3}$ Å) |
|---|---|---|---|---|---|---|
| Al-Ga-P | 2.367 | −1.832±0.009 | −0.09±0.01 | 2.360 | 2.07±0.01 | −0.18±0.01 |
| Al-Ga-As | 2.451 | −0.948±0.004 | 0.164±0.006 | 2.448 | 0.891±0.004 | −0.038±0.006 |
| Al-Ga-Sb | 2.656 | −4.11±0.02 | −0.20±0.03 | 2.640 | 4.62±0.02 | −0.18±0.03 |
| Al-In-P | 2.367 | 54.6±0.2 | −19.3±0.3 | 2.541 | −29.9±0.2 | −18.4±0.3 |
| Al-In-As | 2.451 | 61.3±0.2 | −27.7±0.4 | 2.622 | −28.5±0.2 | −28.2±0.3 |
| Al-In-Sb | 2.656 | 49.8±0.2 | −22.1±0.3 | 2.805 | −24.5±0.2 | −22.4±0.3 |
| Ga-In-P | 2.360 | 61.1±0.3 | −24.3±0.4 | 2.541 | −30.8±0.2 | −24.0±0.3 |
| Ga-In-As | 2.448 | 58.64±0.06 | −22.64±0.09 | 2.622 | −31.01±0.06 | −23.53±0.07 |
| Ga-In-Sb | 2.640 | 57.7±0.2 | −25.2±0.3 | 2.805 | −28.4±0.2 | −25.4±0.3 |
| Al-P-As | 2.367 | 24.5±0.1 | −1.6±0.2 | 2.451 | −22.8±0.1 | −0.9±0.2 |
| Al-P-Sb | 2.367 | 109.4±0.4 | −47.9±0.6 | 2.656 | −44.1±0.4 | −48.6±0.6 |
| Al-As-Sb | 2.451 | 75.2±0.3 | −28.7±0.4 | 2.656 | −39.4±0.3 | −29.2±0.4 |
| Ga-P-As | 2.360 | 28.5±0.1 | −6.0±0.2 | 2.448 | −22.1±0.1 | −5.7±0.2 |
| Ga-P-Sb | 2.360 | 114.8±0.4 | −53.4±0.6 | 2.640 | −45.4±0.4 | −56.7±0.6 |
| Ga-As-Sb | 2.448 | 69.2±0.3 | −22.6±0.4 | 2.640 | −40.9±0.3 | −22.4±0.4 |
| In-P-As | 2.541 | 21.06±0.09 | −5.5±0.1 | 2.622 | −15.2±0.1 | −5.0±0.1 |
| In-P-Sb | 2.541 | 92.8±0.3 | −50.3±0.4 | 2.805 | −25.8±0.3 | −53.9±0.5 |
| In-As-Sb | 2.622 | 56.7±0.2 | −22.4±0.3 | 2.805 | −28.5±0.2 | −22.2±0.3 |
| Zn-Hg-S | 2.342 | 45.9±0.2 | −24.9±0.3 | 2.534 | −10.7±0.1 | −23.3±0.2 |
| Zn-Hg-Se | 2.454 | 41.9±0.2 | −19.5±0.3 | 2.634 | −15.2±0.1 | −16.7±0.2 |
| Zn-Hg-Te | 2.637 | 42.3±0.2 | −19.4±0.3 | 2.798 | −18.2±0.1 | −18.2±0.2 |
| Zn-Cd-Te | 2.637 | 43.8±0.2 | −20.5±0.3 | 2.806 | −17.8±0.1 | −19.3±0.2 |
| Cd-Hg-Te | 2.806 | −1.017±0.007 | −0.14±0.01 | 2.798 | 1.497±0.007 | −0.33±0.01 |
| Zn-S-Se | 2.342 | 26.0±0.1 | −8.7±0.2 | 2.454 | −15.1±0.1 | −8.1±0.2 |
| Zn-S-Te | 2.342 | 92.0±0.3 | −43.0±0.4 | 2.656 | −125.1±0.3 | 54.6±0.5 |
| Zn-Se-Te | 2.454 | 46.6±0.2 | −10.7±0.3 | 2.637 | −30.0±0.2 | −7.8±0.3 |
| Hg-S-Se | 2.534 | 15.06±0.07 | −4.7±0.1 | 2.634 | −8.92±0.07 | −3.2±0.1 |
| Hg-S-Te | 2.534 | 63.4±0.2 | −32.5±0.3 | 2.798 | −11.6±0.2 | −28.9±0.3 |
| Hg-Se-Te | 2.634 | 31.4±0.1 | −10.9±0.2 | 2.798 | −14.9±0.1 | −8.7±0.2 |

TABLE III. Quadratic parameters for common sublattice NNN distances [Eqs. (3) and (4)].

| $A_xB_{1-x}C$ / $CA_xB_{1-x}$ | $\bar{R}_{CAC}[f(1-x)]$ | | | $\bar{R}_{CBC}[f(x)]$ | | |
|---|---|---|---|---|---|---|
| | $R^0$ (Å) | $b$ ($10^{-3}$ Å) | $c$ ($10^{-3}$ Å) | $R^0$ (Å) | $b$ ($10^{-3}$ Å) | $c$ ($10^{-3}$ Å) |
| Al-Ga-P | 3.865 | −2.91±0.04 | −0.33±0.06 | 3.854 | 3.46±0.04 | −0.43±0.06 |
| Al-Ga-As | 4.002 | −1.42±0.02 | 0.10±0.02 | 3.998 | 1.43±0.02 | 0.09±0.02 |
| Al-Ga-Sb | 4.337 | −6.69±0.09 | −0.4±0.1 | 4.311 | 7.58±0.09 | −0.4±0.1 |
| Al-In-P | 3.865 | 85±1 | −28±1 | 4.149 | −54±1 | −25±2 |
| Al-In-As | 4.002 | 97.2±0.9 | −42±1 | 4.282 | −51±1 | −42±2 |
| Al-In-Sb | 4.337 | 78.9±0.8 | −34±1 | 4.580 | −43.1±0.9 | −33±1 |
| Ga-In-P | 3.854 | 96.2±1.0 | −36±1 | 4.149 | −56±1 | −34±2 |
| Ga-In-As | 3.998 | 92.5±0.2 | −33.6±0.3 | 4.282 | −55.2±0.3 | −33.7±0.4 |
| Ga-In-Sb | 4.311 | 91.4±0.9 | −38±1 | 4.580 | −50±1 | −38±1 |
| Al-P-As | 3.865 | 39.2±0.5 | −1.92±0.7 | 4.002 | −38.0±0.5 | −0.6±0.7 |
| Al-P-Sb | 3.865 | 169±2 | −69±2 | 4.337 | −83±2 | −68±3 |
| Al-As-Sb | 4.002 | 119±1 | −43±2 | 4.337 | −70±1 | −42±2 |
| Ga-P-As | 3.854 | 45.8±0.5 | −9.3±0.7 | 3.998 | −36.9±0.5 | −8.4±0.7 |
| Ga-P-Sb | 3.854 | 180±1 | −80±2 | 4.311 | −83±2 | −83±2 |
| Ga-As-Sb | 3.998 | 109±1 | −33±1 | 4.311 | −71±1 | −32±2 |
| In-P-As | 4.149 | 33.4±0.5 | −7.9±0.7 | 4.282 | −26.1±0.5 | −7.1±0.7 |
| In-P-Sb | 4.149 | 143±1 | −73±2 | 4.580 | −53±2 | −77±2 |
| In-As-Sb | 4.282 | 88±1 | −32±2 | 4.580 | −51±1 | −31±2 |
| Zn-Hg-S | 3.824 | 68±1 | −33±2 | 4.138 | −27±1 | −28±2 |
| Zn-Hg-Se | 4.007 | 63±1 | −26±2 | 4.301 | −33±1 | −19±2 |
| Zn-Hg-Te | 4.306 | 65.3±1.0 | −28±1 | 4.569 | −35±1 | −24±2 |
| Zn-Cd-Te | 4.306 | 68±1 | −30±1 | 4.582 | −35±1 | −25±2 |
| Cd-Hg-Te | 4.582 | −1.75±0.05 | −0.15±0.08 | 4.569 | 2.27±0.05 | −0.36±0.08 |
| Zn-S-Se | 3.824 | 40.3±0.7 | −12±1 | 4.007 | −27.5±0.7 | −10±1 |
| Zn-S-Te | 3.824 | 135±2 | −55±3 | 4.337 | −227±2 | 117±3 |
| Zn-Se-Te | 4.007 | 70±1 | −12±2 | 4.306 | −54±1 | −8±2 |
| Hg-S-Se | 4.138 | 22.1±0.7 | −5.2±1.0 | 4.301 | −17.2±0.7 | −2±1 |
| Hg-S-Te | 4.138 | 88±2 | −38±3 | 4.569 | −34±2 | −31±3 |
| Hg-Se-Te | 4.301 | 46±1 | −12±2 | 4.569 | −30±1 | −9±2 |

smaller than the number of significant digits provided in Table IV, it is not included.

Several useful pieces of information may be extracted from the parameters for the nearest-neighbor distances, including the bond-length relaxation parameter[15] in the impurity limit,

$$\epsilon_{AC}=\frac{R^i_{AC}-R^0_{BC}}{R^0_{AC}-R^0_{BC}}=\frac{b_{AC}+c_{AC}}{R^0_{AC}-R^0_{BC}}+1\ ,$$
$$\epsilon_{BC}=\frac{R^i_{BC}-R^0_{AC}}{R^0_{BC}-R^0_{AC}}=\frac{b_{BC}+c_{BC}}{R^0_{BC}-R^0_{AC}}+1\ , \tag{5}$$

and the nonlinear bowing coefficients, $-c_{AC}$, $-c_{BC}$, which measure the quadratic dependence on $x$ of $\bar{R}_{AC}$ and $\bar{R}_{BC}$, respectively. Also, the bond length of $AC$ as a dilute impurity in crystalline $BC$ is calculated as $R^i_{AC}=R^0_{AC}+b_{AC}+c_{AC}$. The impurity limits for second-neighbor distances on either the mixed or common sublattice are determined in a similar manner, using the parameters from Tables III and IV. Two values of impurity bond length may be derived for $\bar{R}_{ACB}$, one corresponding to $x=0$, $\bar{R}^0_{ACB}$, and the other to $x=1$, $\bar{R}^0_{ACB}+b_{ACB}+c_{ACB}$.

The present work extends that done analytically by Martins and Zunger,[15] who allowed breathing mode relaxation of two shells surrounding an isolated impurity atom. Other workers have noted[13,16] that this method tends to overestimate the magnitude of the impurity bond-length relaxation. Comparison of our results for $Ga_xIn_{1-x}As$ of $R^i_{GaAs}=2.484$ Å and $R^i_{InAs}=2.567$ Å [calculated from Eqs. (3) and (4)] with their values of 2.495 and 2.556 Å shows this to be true. That this effect arises from the small relaxation radius about the impurity and is not due to inaccuracies in the model is demonstrated by the results of the current simulation.

The first-neighbor bond-length distributions for $Ga_{0.05}In_{0.95}As$ through $Ga_{0.50}In_{0.50}As$ are plotted in Fig. 4. Examination of these reveals a slightly asymmetric, but clearly unimodal peak for both Ga—As and In—As bonds, in agreement with previous observations.[13,14] As the supercell composition approaches $Ga_{0.50}In_{0.50}As$, the individual distributions broaden significantly. This is a consequence of an increasingly inhomogeneous chemical environment in mixed sublattice shells surrounding the atoms at the ends of the bond, leading to a maximum width at $x=0.50$. For $x>0.50$, the behavior of the bond-length distributions is analogous to that seen in Fig. 4, with the Ga-As distribution narrowing and growing dominant as $x\to 1$. Analysis of the functional dependence of peak width ($\bar{\Gamma}$) on compositions shows a strong correlation of the form

TABLE IV. Quadratic parameters for mixed sublattice NNN distances [Eqs. (3) and (4)].

| $A_xB_{1-x}C$ | | $\bar{R}_{ACA}[f(1-x)]$ | | | $\bar{R}_{BCB}[f(x)]$ | | | $\bar{R}_{ACB}[f(x)]$ | |
|---|---|---|---|---|---|---|---|---|---|
| $CA_xB_{1-x}$ | $R^0$ (Å) | $b$ ($10^{-3}$ Å) | $c$ ($10^{-3}$ Å) | $R^0$ (Å) | $b$ ($10^{-3}$ Å) | $c$ ($10^{-3}$ Å) | $R^0$ (Å) | $b$ ($10^{-3}$ Å) | $c$ ($10^{-3}$ Å) |
| Al-Ga-P | 3.865 | −8.18±0.04 | −0.66±0.06 | 3.854 | 8.88±0.03 | −0.72±0.06 | 3.855 | 9.75±0.09 | −1.35±0.06 |
| Al-Ga-As | 4.002 | −3.68±0.03 | 0.03±0.02 | 3.998 | 3.64±0.01 | 0.11±0.02 | 3.998 | 3.26±0.02 | 0.39±0.05 |
| Al-Ga-Sb | 4.337 | −18.98±0.09 | −0.7±0.1 | 4.311 | 19.93±0.08 | −0.94±0.01 | 4.314 | 20.9±0.1 | −1.5±0.3 |
| Al-In-P | 3.865 | 213.6±0.9 | −23±1 | 4.149 | −197.2±0.9 | −25±1 | 4.106 | −187±2 | −18±3 |
| Al-In-As | 4.002 | 216.6±0.8 | −34±1 | 4.282 | −193.6±0.9 | −35±1 | 4.239 | −174±2 | −31±3 |
| Al-In-Sb | 4.337 | 185.1±0.8 | −25±1 | 4.580 | −169.2±0.8 | −25±1 | 4.543 | −156±2 | −21±3 |
| Ga-In-P | 3.854 | 226.5±0.9 | −31±1 | 4.149 | −204±1 | −34±1 | 4.104 | −188±3 | −27±3 |
| Ga-In-As | 3.998 | 220.8±0.2 | −32.8±0.2 | 4.282 | −198.9±0.2 | −31.5±0.2 | 4.237 | −169.2±0.5 | −39.1±0.5 |
| Ga-In-Sb | 4.311 | 207.3±0.8 | −30±1 | 4.580 | −187.7±0.9 | −30±1 | 4.539 | −171±2 | −26±3 |
| Al-P-As | 3.865 | 100.9±0.4 | 1.8±0.7 | 4.002 | −103.2±0.4 | 2.1±0.5 | 3.985 | −107±1 | 5±1 |
| Al-P-Sb | 3.865 | 365±1 | −48±2 | 4.337 | −327±1 | −52±2 | 4.266 | −305±4 | −41±5 |
| Al-As-Sb | 4.002 | 259±1 | −30±2 | 4.337 | −237±1 | −33±1 | 4.289 | −223±3 | −25±3 |
| Ga-P-As | 3.854 | 108.6±0.4 | −4.7±0.7 | 3.998 | −106.3±0.4 | −4.6±0.5 | 3.978 | −105±1 | −2±1 |
| Ga-P-Sb | 3.854 | 361±1 | −53±2 | 4.311 | −320±1 | −56±2 | 4.244 | −294±4 | −47±5 |
| Ga-As-Sb | 3.998 | 240.6±0.9 | −19±2 | 4.311 | −226.7±0.9 | −20±1 | 4.268 | −221±2 | −13±3 |
| In-P-As | 4.149 | 95.0±0.5 | −3.3±0.7 | 4.282 | −93.5±0.4 | −4.0±0.6 | 4.262 | −94±1 | 0±2 |
| In-P-Sb | 4.149 | 327±1 | −52±2 | 4.580 | −288±1 | −55±2 | 4.511 | −265±4 | −43±5 |
| In-As-Sb | 4.282 | 222±1 | −21±2 | 4.580 | −207±1 | −23±1 | 4.535 | −200±3 | −14±3 |
| Zn-Hg-S | 3.824 | 223±1 | −38±2 | 4.138 | −196±1 | −43±2 | 4.080 | −176±3 | −34±4 |
| Zn-Hg-Se | 4.007 | 210±1 | −32±2 | 4.301 | −189±1 | −34±2 | 4.249 | −171±3 | −28±4 |
| Zn-Hg-Te | 4.306 | 191.8±0.9 | −28±2 | 4.569 | −173±1 | −29±1 | 4.524 | −159±3 | −23±3 |
| Zn-Cd-Te | 4.306 | 201±1 | −32±2 | 4.582 | −181±1 | −32±1 | 4.534 | −163±3 | −27±4 |
| Cd-Hg-Te | 4.582 | −8.67±0.06 | −0.34±0.09 | 4.569 | 9.09±0.05 | −0.05±0.06 | 4.571 | 9.4±0.1 | −0.6±0.2 |
| Zn-S-Se | 3.824 | 128.9±0.7 | −7±1 | 4.007 | −124.5±0.7 | −7.0±0.8 | 3.978 | −123±2 | −3±2 |
| Zn-S-Te | 3.824 | 352±2 | −37±3 | 4.337 | −444±2 | 66±2 | 4.228 | −324±5 | −12±6 |
| Zn-Se-Te | 4.007 | 213±1 | −5±2 | 4.306 | −209±1 | −4±1 | 4.261 | −213±3 | −3±4 |
| Hg-S-Se | 4.138 | 108.0±0.7 | −4±1 | 4.301 | −106.3±0.7 | 3.0±0.9 | 4.272 | −107±2 | 0±2 |
| Hg-S-Te | 4.138 | 300±2 | −28±3 | 4.569 | −274±2 | −27±2 | 4.493 | −273±5 | −13±6 |
| Hg-Se-Te | 4.301 | 181±1 | −5±2 | 4.569 | −176±1 | −4±1 | 4.524 | −181±3 | 3±4 |

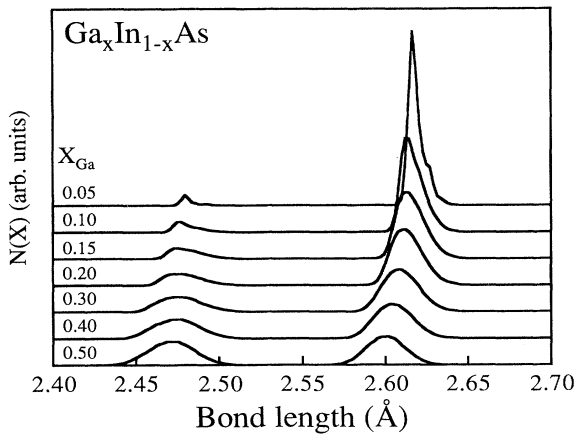


FIG. 4. Distribution functions for the Ga—As and In—As bond lengths are shown for compositions in the range $0.05 < x < 0.50$. Both peaks are seen to broaden systematically as $x \rightarrow 0.50$.

$$\bar{\Gamma}^2 = 4\Gamma_0^2 x(1-x) . \quad (6)$$

We provide parameters for the intrinsic peak widths of the bond-length distributions ($AC$) and ($BC$) in Table V. The parameter $\bar{\Gamma}$ represents additional broadening of the distributions of first-neighbor distances beyond the Debye-Waller factor. While this excess broadening of the spectra for $Ga_xIn_{1-x}As$ was not observed,[3,4] the stated upper limit on additional broadening of 0.02 Å is very nearly equal to our predicted maximum widths for the Ga-As and In-As distributions (0.025 and 0.021 Å, respectively). Also the discovery that the Ga-As and In-As distributions have the same width to within ±0.01 Å does not contradict our result ($\bar{\Gamma}_{InAs} - \bar{\Gamma}_{GaAs} = 0.004$ Å). Of the systems studied, these effects are still quite small for the most strained systems ($\bar{\Gamma} \approx 0.039$ Å for $AlP_xSb_{1-x}$ and $\bar{\Gamma} \approx 0.041$ Å for $GaP_xSb_{1-x}$), where this additional broadening would be most easily observed.

The distributions of second-neighbor distances cannot be described solely in terms of their mean values and peak widths because they are multimodal, unlike the dis-

TABLE V. Quadratic parameters for bond distribution widths [Eq. (6)].

| $A_xB_{1-x}C$ $CA_xB_{1-x}$ | $\Gamma^2_{0AC}$ ($10^{-7}$ Å$^2$) | $\Gamma^2_{0BC}$ ($10^{-7}$ Å$^2$) | $A_xB_{1-x}C$ $CA_xB_{1-x}$ | $\Gamma^2_{0AC}$ ($10^{-7}$ Å$^2$) | $\Gamma^2_{0BC}$ ($10^{-7}$ Å$^2$) |
|---|---|---|---|---|---|
| Al-Ga-P | 9.0±0.4 | 10.8±0.5 | Zn-Hg-S | 3500±200 | 1730±80 |
| Al-Ga-As | 1.95±0.09 | 1.99±0.09 | Zn-Hg-Se | 3700±200 | 1660±80 |
| Al-Ga-Sb | 46±2 | 57±2 | Zn-Hg-Te | 3400±200 | 2200±100 |
| Al-In-P | 5800±300 | 4100±200 | Zn-Cd-Te | 3800±200 | 2100±100 |
| Al-In-As | 6700±300 | 5200±20 | Cd-Hg-Te | 4.4±0.2 | 5.2±0.2 |
| Al-In-Sb | 3900±200 | 3700±200 | Zn-S-Se | 1170±60 | 1430±70 |
| Ga-In-P | 7100±300 | 4500±200 | Zn-S-Te | 8800±400 | 10 900±500 |
| Ga-In-As | 6290±80 | 4480±60 | Zn-Se-Te | 4000±200 | 4300±200 |
| Ga-In-Sb | 5500±300 | 4500±200 | Hg-S-Se | 460±20 | 480±20 |
| Al-P-As | 1320±60 | 1610±80 | Hg-S-Te | 3500±200 | 4900±200 |
| Al-P-Sb | 15 500±700 | 15 200±700 | Hg-Se-Te | 1420±70 | 1990±90 |
| Al-As-Sb | 9300±400 | 7900±400 | | | |
| Ga-P-As | 1620±80 | 1700±80 | | | |
| Ga-P-Sb | 16 100±800 | 16 800±800 | | | |
| Ga-As-Sb | 7700±400 | 8000±400 | | | |
| In-P-As | 870±40 | 1040±50 | | | |
| In-P-Sb | 9000±400 | 11 400±500 | | | |
| In-As-Sb | 4900±200 | 5400±300 | | | |

tributions of first neighbors. In particular, the common sublattice second-neighbor distributions in $A_xB_{1-x}C$ clearly exhibit trimodal character, while those of the mixed sublattice are broadened and non-Gaussian in form. The dependence of these functions on environment is attributed primarily to variations in the first- and second-neighbor shells around the atom at the vertex of the bond angle. This assumption allows identification of three independent and distinct environments for each of the five second-neighbor distributions. Schematic illustrations of the relevant configurations for arbitrary second-neighbor distributions on both the mixed and common sublattices are presented in Fig. 5. In order to simplify the description of effects leading to splitting in the NNN distributions, we will discuss the $A$-$C$-$A$ distance on the mixed sublattice and the $C$-$A$-$C$ distance on the common sublattice. For the purposes of this section, the behavior of the $A$-$C$-$B$ and $B$-$C$-$B$ distributions is identical to that of $A$-$C$-$A$, and $C$-$B$-$C$ is equivalent to $C$-$A$-$C$. On the mixed sublattice, the primary distortions are the result of inhomogeneities in the first-neighbor shell. Occupying any $C$ centered tetrahedron with an $A$-$C$-$A$ bond angle are four atoms from the mixed sublattice, at least two of which are of type $A$. Thus, the three possible arrangements of atoms around the central $C$ atom are $A_4$, $A_3B$, and $A_2B_2$. Because of bond-length alternation in the alloy lattice, we expect each of these tetrahedra, shown in Fig. 5, to distort in a slightly different manner. Clearly, the greatest distortion will occur in $A_2B_2$, where the two $B$-$C$ bonds will strongly influence the central atom. Similarly, the $A_4$ configuration will distort the least, remaining closer to the ideal VCA second-neighbor distance for the compound $AC$, while the $A_3B$ tetrahedron will experience a distortion intermediate between these two extremes. In contrast with the $A$-$C$-$A$ second-neighbor distribution, the $C$-$A$-$C$ NNN distance is primarily influenced by an

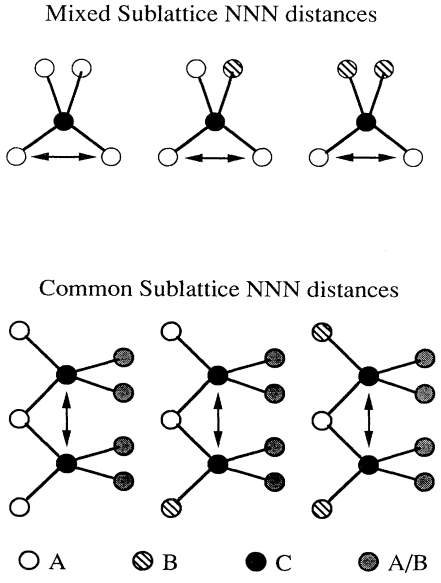


FIG. 5. The local environments responsible for splitting in NNN distance distributions are illustrated schematically for both the mixed and common sublattices. An arrow is used to denote the relevant second-neighbor pairs in each diagram. For the $A$-$A$ NNN distance ($\bar{R}_{ACA}$) on the mixed sublattice, the three peaks comprising the overall distribution arise from the $A_4$, $A_3B$, and $A_2B_2$ configurations surrounding the central $C$ atom. The geometries of each of these are diagrammed in the top part of the figure. In contrast, the common sublattice NNN distributions arise from the arrangement of atoms in the second-neighbor shell around the central $A$ or $B$ atom. Of the many potential configurations of these atoms, those involving permutations of the two lying on the chains in ⟨110⟩ directions are crucial. Atoms shaded in gray are those on the mixed sublattice which are less important in determining the NNN distances.

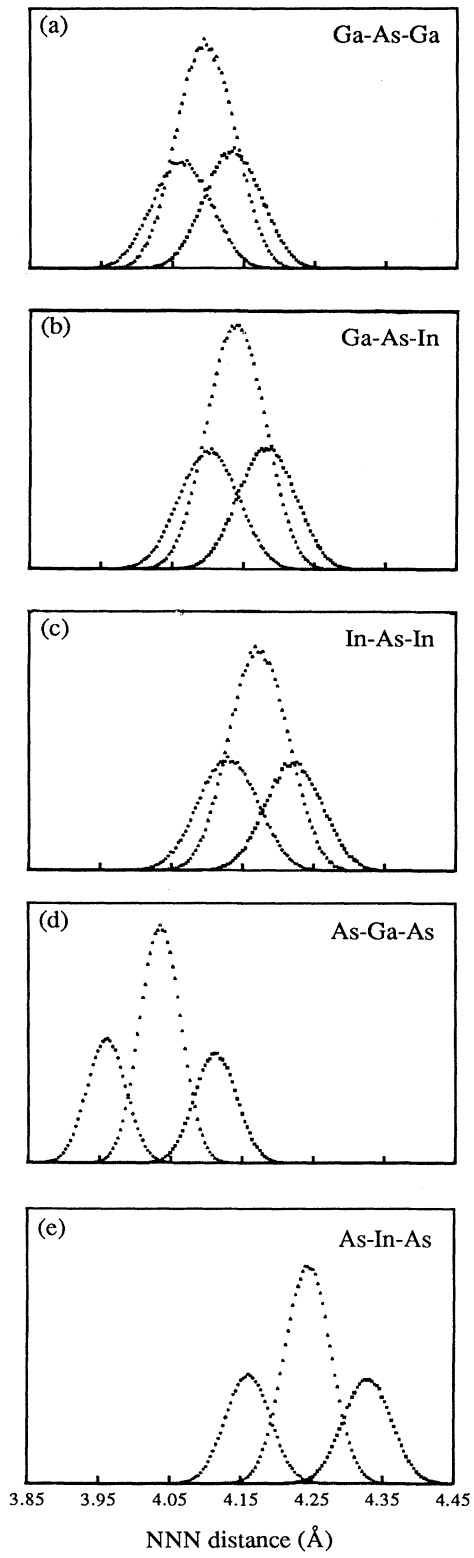


FIG. 6. Distributions of second-neighbor distances for $Ga_{0.50}In_{0.50}As$ are shown for the five NNN types in panels (a) through (e). In each panel the distributions are further broken down into three components associated with the geometrical configurations shown in Fig. 5.

inhomogeneous cation environment in the second-neighbor shell. Fortunately, the number of atomic configurations in this shell about the vertex atom may be reduced from $\binom{4}{2}$ possible arrangements to three configurations of the atoms lying on chains in $\langle 110 \rangle$ directions. This is emphasized in Fig. 5 by shading gray those atoms in the second-neighbor shell which do not lie in the plane of the bond angle. Again, the $C$-$A$-$C$ distribution splits into three peaks, one each for the $A_2$, $AB$, and $B_2$ configurations, with the distortions occurring in a fashion similar to those for $A$-$C$-$A$. Figure 6 shows distributions for each of the five second-neighbor types, separated into the three components described above. Distribution functions for each of the configurations in Fig. 5 were obtained by accumulating second-neighbor distances in relaxed 216-atom supercells of $Ga_{0.50}In_{0.50}As$ over 2500 random cell reconfigurations. Association of each subsidiary peak with a specific first- (mixed sublattice) or second-neighbor (common sublattice) environment about the atom at the center of the bond angle is shown to be an excellent approximation by the absence of significant skewness or other deviation of the distributions from Gaussian form.

Inspection of Fig. 6 reveals substantially greater splitting between individual distribution peaks for the As-As NNN distributions than for the cation-cation distributions. Examination of the geometries shown schematically in Fig. 5 shows the cause of this behavior. If it is assumed, for the sake of argument, that any distortion which requires compression or dilation of a bond will be accompanied by a corresponding bending of the adjacent bond angles, we recognize the strong dependence of distortions around an atom on the orientation of forces acting on it. In the mixed sublattice, splitting in NNN distributions arises from the influence of two inhomogeneous atoms acting normal to the plane of bond angle, while the forces on a second-neighbor pair in the common sublattice act in this plane. As a result, changes in bond lengths in the mixed sublattice have a smaller effect on the associated second-neighbor pair than do similar changes in the common sublattice.

The energies of alloy formation and stability are of significant interest in studies of these systems.[14,20–27] If chemical interaction energies are neglected as in the Keating model, it is clear that phase segregation is the favored behavior in all strained alloy supercells at low temperature. However, the existence of ordered structures which provide metastable configurations of minimum strain energy is a question which has relevance when chemical energies are considered, as well as being of interest in total energy calculations.[11,26,27] While a thermodynamic treatment of this topic lies outside the scope of the present work, a number of interesting observations may be made regarding the correlation of total strain energy for a given supercell configuration and the average properties of that supercell. In Fig. 7 we show a scatter plot revealing linear variation of average bond length for Ga—As and In—As bonds with strain energy. In this diagram, each point represents the relationship between supercell energy and the average bond lengths of the constituent compounds for one specific configuration.

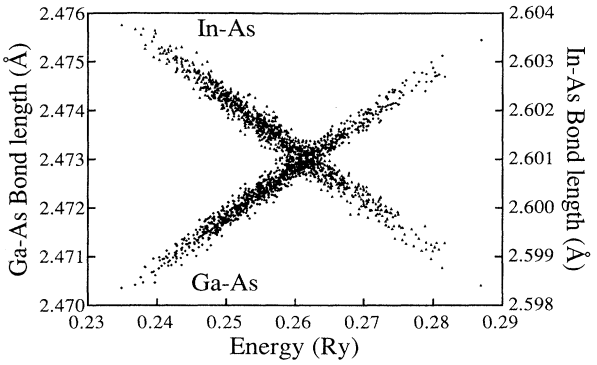


FIG. 7. This scatter plot shows the strong linear correlation between average Ga—As and In—As bond lengths and supercell strain energy for $Ga_{0.50}In_{0.50}As$. Each point on the plot represents the average values of bond length for a single configuration as compared with the energy of that configuration. As expected, a direct correlation is seen between the average distortion of the lattice and the energy associated with that distortion.

As expected, a direct correlation between the extent to which a lattice geometry is energetically favorable and the closeness of the average bond lengths in the supercell to their ideal end-point values is clearly shown. The extent to which this elastic energy plays a role in the formation of alloys varies widely among the compounds, depending primarily on the difference in bond lengths between the two constituents. For example, the order-disorder transition temperature for the systems studied, calculated using the site approximation for configurational entropy,[21] ranges from a low of $2U/k \approx 1.4\times10^{-1}$ K for $Al_{0.50}Ga_{0.50}As$ to a high of $2U/k \approx 1.2\times10^{3}$ K for $GaP_{0.50}Sb_{0.50}$.

## IV. CONCLUSIONS

We conclude the following from the results of our valence-force-field simulation of relaxation in pseudobinary semiconductor alloys. (i) Distortion of both fcc sublattices occurs to an appreciable degree. The common sublattice experiences deviation from zinc-blende sites as a consequence of an inhomogeneous first-neighbor shell, while the mixed sublattice distorts primarily due to variation in the second-neighbor shell. Significantly greater average distortion is seen on the common sublattice, as expected for atoms with substantial variation in the near-neighbor environment. (ii) Experimental EXAFS results are reproduced very well in our Keating VFF simulations. The variation of bond lengths and second-neighbor distances with composition is predicted within error bars for $Ga_xIn_{1-x}As$, with some deviation arising for the In-As distance due to previously noted uncertainties in the model parameters for this compound. (iii) Both NN and NNN distances are well described by a quadratic dependence on composition. Parameters are provided for fits to data from eighteen III-V and eleven II-VI systems, allowing prediction of these quantities for any alloy composition and for alloys for which there are no experimental results. (iv) The intrinsic broadening of alloy bond-length distributions is quantitatively predicted. This additional broadening of first-neighbor distributions is found to vary with alloy composition as $\overline{\Gamma}^2 = 4\Gamma_0^2 x(1-x)$. Values of the parameter $\Gamma_0^2$ are tabulated for all alloy systems studied, enabling estimation of the significance of this effect. (v) Distributions of NNN distances are found to show trimodal splitting arising from variation in the local environment. Second-neighbor distributions on the common sublattice exhibit the greatest splitting magnitude between the three individual peaks. This is attributed to elongation or compression along ⟨110⟩ chains including the second-neighbor pair. Smaller, but still significant, splitting is seen in NNN distributions on the mixed sublattice. Here, the second-neighbor distance varies with the configuration of atoms surrounding the vertex atom. Because the first shell around each atom on the mixed sublattice is uniformly occupied, the distortion experienced by these second-neighbor pairs is decreased.

## ACKNOWLEDGMENTS

Computational resources for this study were provided by the Minnesota Supercomputer Institute.

[1]For a review of the properties of semiconductor alloys see *GaInAsP Alloy Semiconductors,* edited by T. P. Pearsall (Wiley, New York, 1982); J. C. Woolley, in *Compound Semiconductors,* edited by R. K. Williardson and H. L. Goering (Reinhold, New York, 1962); H. C. Casey and M. B. Panish, *Heterostructure Lasers* (Academic, New York, 1978); M. Jaros, Rep. Prog. Phys. **48**, 1091 (1985).

[2]L. Vegard, Z. Phys. **5**, 17 (1921); J. C. Wooley, and B. C. Smith, Proc. Phys. Soc. London **72**, 241 (1958).

[3]J. C. Mikkelsen and J. B. Boyce, Phys. Rev. Lett. **49**, 1412 (1982).

[4]J. C. Mikkelsen and J. B. Boyce, Phys. Rev. B **28**, 7130 (1983).

[5]A. Balzarotti, A. Kisiel, N. Motta, M. Zimnal-Starnawska, M. T. Czyżyk, and M. Podgòrny, Phys. Rev. B **30**, 2295 (1984); A. Balzarotti, N. Motta, A. Kisiel, M. Zimnal-Starnawska, M. T. Czyżyk, and M. Podgòrny, *ibid.* **31**, 7526 (1985).

[6]J. C. Mikkelsen and J. B. Boyce, in *Proceedings of the XVII International Conference on the Physics of Semiconductors,* edited by J. D. Chadi and W. A. Harrison (Springer-Verlag, New York, 1985), p. 933.

[7]N. Motta, A. Balzarotti, P. Letardi, A. Kisiel, M. T. Czyżyk, M. Zimnal-Starnawska, and M. Podgòrny, Solid State Commun. **53**, 509 (1985).

[8]H. Oyanagi, Y. Takedo, T. Matsushita, T. Ishiguro, T. Yao, and A. Sasaki, Solid State Commun. **67**, 453 (1988).

[9]A. Zunger and J. E. Jaffe, Phys. Rev. Lett. **51**, 662 (1983).

[10]K. C. Hass, R. J. Lemperd, and H. Ehrenreich, Phys. Rev. Lett. **52**, 77 (1984).

[11]A. Zunger, S-H. Wei, L. G. Ferreira, and J. E. Bernard, Phys. Rev. Lett. **65**, 353 (1990).
[12]P. N. Keating, Phys. Rev. **145**, 637 (1966); R. M. Martin, Phys. Rev. B **1**, 4005 (1970).
[13]M. Podgòrny, M. T. Czyżyk, A. Balzarotti, P. Letardi, N. Motta, A. Kisiel, and M. Zimnal-Starnawska, Solid State Commun. **55**, 413 (1985).
[14]A. Qteish, N. Motta, and A. Balzarotti, Phys. Rev. B **39**, 5987 (1989).
[15]J. L. Martins and A. Zunger, Phys. Rev. B **30**, 6217 (1984).
[16]A-B. Chen and A. Sher, Phys. Rev. B **32**, 3695 (1985).
[17]T. Fukui, J. Appl. Phys. **57**, 5188 (1985); C. K. Shih, W. E. Spicer, W. A. Harrison, and A. Sher, Phys. Rev. B **31**, 1139 (1985).
[18]W. H. Press, B. P. Flannery, S. A. Teukolsky, and W. T. Vetterling, *Numerical Recipes: The Art of Scientific Computing* (Cambridge University Press, New York, 1986).
[19]M-H. Tsai, J. D. Dow, and K. E. Newman, Phys. Rev. B **41**, 7744 (1990).
[20]P. Boguslawski and A. Baldereschi, Solid State Commun. **66**, 679 (1988).
[21]B. Koiller and M. O. Robbins, Phys. Rev. B **40**, 12 554 (1989).
[22]A. A. Mbaye, Solid State Commun. **55**, 183 (1985).
[23]A. Sher, M. van Schilfgaarde, A-B. Chen, and W. Chen, Phys. Rev. B **36**, 4279 (1987).
[24]A. A. Mbaye, D. M. Wood, and A. Zunger, Phys. Rev. B **37**, 3008 (1988).
[25]S. Lee, D. M. Bylander, and L. Kleinman, Phys. Rev. B **40**, 8399 (1989).
[26]G. P. Srivastava, J. L. Martins, and A. Zunger, Phys. Rev. B **31**, 2561 (1985).
[27]J. L. Martins and A. Zunger, Phys. Rev. B **32**, 2689 (1985).